EUROPHYSICS LETTERS 15 March 2000

Europhys. Lett., **49** (6), pp. 722–728 (2000)

Novel structural features of the ripple phase of phospholipids

K. Sengupta[1], V. A. Raghunathan[1] and J. Katsaras[2]

[1] *Raman Research Institute - Bangalore, 560 080, India*
[2] *National Research Council, Steacie Institute of Molecular Sciences Chalk River Laboratories - Chalk River, Ontario K0J 1J0, Canada*

(received 28 June 1999; accepted in final form 13 January 2000)

PACS. 61.10.Eq – X-ray scattering (including small-angle scattering).
PACS. 61.30.Eb – Experimental determinations of smectic, nematic, cholesteric, and other structures.

Abstract. – We have calculated, from X-ray diffraction data, the electron density maps of the ripple phase of dimyristoylphosphatidylcholine (DMPC) and palmitoyl-oleoyl phosphatidylcholine (POPC) multibilayers at different temperatures and fixed relative humidity. Our analysis of the maps establishes the existence of an average tilt of the hydrocarbon chains of the lipid molecules along the direction of the ripple wave vector, which we believe is responsible for the occurrence of asymmetric ripples in these systems.

Lipids self-assemble in water to form a variety of lamellar phases [1, 2]. The ripple or $P_{\beta'}$ phase characterized by a one-dimensional height modulation of the bilayers is seen in some phospholipids under high hydration [1,3]. In the phase diagrams of these systems, it is sandwiched between the high-temperature L_α phase and the low-temperature $L_{\beta'}$ phase [2,3]. In the L_α phase, the hydrocarbon chains of the lipid molecules are in a molten state and the in-plane ordering is liquid-like. On the other hand, in the $L_{\beta'}$ phase, the chains are predominantly in the all-*trans* conformation and are tilted with respect to the layer normal. The chains are also ordered in the plane of the bilayer, but it is not yet clear whether the in-plane ordering is crystalline or hexatic [1, 2].

Experimental studies on the ripple phase have established many of its structural features. Almost all X-ray studies show asymmetric ripples corresponding to an oblique unit cell of the rippled bilayers [1,3–5]; though there have been some reports of symmetric ripples corresponding to a rectangular unit cell [6, 7]. The latter have been shown to be metastable structures in some systems [7]. It is well established that only lipids that have an $L_{\beta'}$ phase at lower temperatures exhibit the ripple phase, indicating the importance of the tilt of the chains in the formation of the ripples [8]. Determination of the chain tilt in the ripple phase is of utmost relevance as it is the key structural feature hitherto unknown. But it has not been possible to obtain it directly from X-ray diffraction patterns as the chain reflections are rather diffuse, probably due to the presence of disordered chains, *i.e.*, chains that are not entirely in the *trans* conformation. NMR and diffusion experiments also detect a population of disordered chains

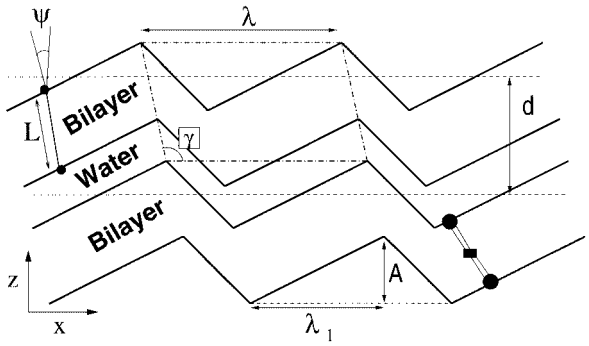

Fig. 1 – Schematic showing the structural parameters of the ripple phase.

in this phase [9, 10]. Hence detailed information about chain tilt has to be deduced from the electron density map of the system, calculated from X-ray diffraction data.

The lack of knowledge of its structural features has hindered the formulation of a satisfactory theory of the ripple phase; none of the current theories is consistent with all the experimental observations. The most striking disagreement concerns the occurrence of asymmetric ripples. It has been proposed that molecular chirality is responsible for such ripples [11], but experiments indicate otherwise [4, 12].

Recently, Sun *et al.* [13] have calculated the electron density map of the ripple phase of DMPC using the X-ray data of Wack and Webb [5]. They find that the ripples have a saw-tooth shape, with the bilayer thickness in the minor arm being much smaller than that in the major arm. Further, the electron density in the headgroup region along the major arm is much higher than that along the minor arm. This led them to hypothesize that the chain organization in the major arm is like in the $L_{\beta'}$ phase and that in the minor arm is like in the L_α phase. However, this conjecture is not supported by other experiments. For example, self-diffusion in the ripple phase is found to be highly anisotropic, with a fast component that is 4-5 orders of magnitude faster than the slow component [10]; but the fast component itself is about 2-3 orders of magnitude smaller than that in the L_α phase. Thus the authors of ref. [10] conclude that although the intramolecular hydrocarbon chain disorder may be substantial in the fast bands, the intermolecular order in this region is not like that in the L_α phase.

In view of this discrepancy, we have calculated the electron density maps of the ripple phase of DMPC and POPC. The ripple phase of DMPC is well studied and its phase diagram is well known. POPC, unlike DMPC, has a double bond in one of its hydrocarbon chains, resulting in a kink in that chain. We have studied POPC in order to see if this difference in the chain conformation influences the structure of the ripple phase. In addition to the X-ray data of ref. [5], we have used data from oriented samples at different temperatures and fixed relative humidity. We find that the ripples in both these systems have a saw-tooth shape, with the ratio of the lengths of the two arms essentially independent of temperature. If the molecules in the short arm were in the L_α phase, the length of this arm would be expected to increase as the L_α phase is approached from below. This is contrary to what we see. Further, the difference in the bilayer thickness and the electron density in the two arms can be largely accounted for in terms of an average tilt of the chains along the direction of rippling, which we believe is responsible for the occurrence of asymmetric ripples in these systems. These results are clearly important for a satisfactory theoretical description of this phase.

We have adopted the modeling and least-squares fitting procedure developed by Sun *et*

al. [13] to calculate the electron density maps. The unit cell parameters of the two-dimensional oblique lattice are the two vectors $\boldsymbol{a}$ and $\boldsymbol{b}$, and the angle γ. In terms of the ripple wavelength λ and the lamellar spacing d, the two lattice vectors can be expressed as: $\boldsymbol{a} = d\cot\gamma\hat{x}+d\hat{z}$, and $\boldsymbol{b} = \lambda\hat{x}$. Here $\hat{x}$ is the direction of the ripple wave vector and $\hat{z}$ is the direction of the average layer normal (see fig. 1). λ, d, and γ are directly measured from the diffraction pattern. The electron density within the unit cell, $\rho(x,z)$, is described as the convolution of a ripple contour function $C(x,z)$ and the transbilayer electron density profile $T_\psi(x,z)$. $C(x,z) = \delta(z-u(x))$, where $u(x)$ describes the ripple profile and is taken to have the form of a saw-tooth with peak-to-peak amplitude A. λ_1 is the projection of the longer arm of the saw-tooth on the x-axis. $T_\psi(x,z)$ gives the electron density at any point (x,z) along a straight line, which makes an angle ψ with the z-axis. The electron density in the methylene region of the bilayer is close to that of water and is taken as zero.

We have used three models for $T_\psi(x,z)$, two of which are equivalent to the SDF and M1G models of ref. [13]. In model I, it is taken as consisting of two delta-functions with positive coefficients ρ_{H}, corresponding to the headgroup regions separated by a distance L, and a central delta-function with negative coefficient of magnitude ρ_{M}, corresponding to the methyl region *i.e.*, $T_\psi(x,z) = \delta(x+z\tan\psi)\{\rho_{\mathrm{H}}[\delta(z-L\cos\psi)+\delta(z+L\cos\psi)]-\rho_{\mathrm{M}}\delta(z)\}$. The six adjustable parameters in model I are: A, λ_1, ψ, $\rho_{\mathrm{H}}/\rho_{\mathrm{M}}$, L and a normalizing factor. In model II, the delta-functions representing the head and methyl groups are replaced with Gaussians of width σ_{h} and σ_{m}, respectively. The electron density in the minor arm is allowed to be different by a factor f_1 from that in the major arm. The region where the two arms meet is modeled as a wall with an electron density differing by a factor f_2 from the rest of the arm. The wall thickness in this model is fixed at a small value. Thus there are 10 adjustable parameters in this model. It is using these two models that Sun *et al.* [13] find that the bilayer thickness along the local layer normal is different in the two arms of the ripple. But this result is built into these models as the parameter L, which is the thickness of the bilayer along a direction that makes an angle ψ with the z-axis, is taken to be the same in the two arms. Therefore, in model III, we remove this constraint and allow L as well as σ_h, σ_{m} and $\rho_{\mathrm{H}}/\rho_{\mathrm{M}}$ to be different in the two arms of the ripple. Further, the wall between the two arms is taken to have a variable width w. This model has 15 adjustable parameters. Minimization is done by iterative least-squares fitting with respect to six variables at a time [14].

The structure factors at the observed (h,k) values are calculated using each of the above models. These are then compared with the observed structure factors and a chi-square value is obtained, which is subsequently minimized by varying the adjustable parameters in the model. The phase of each of the Bragg reflections is obtained from the structure factors calculated from the converged model. These calculated phases are combined with the observed magnitudes of the structure factors and inverse Fourier transformed to get the electron density map of the system. We have used the X-ray diffraction data of Wack and Webb [5] from powder samples of DMPC as well as our data from oriented films of *l*-DMPC, *dl*-DMPC and POPC. Details of the experimental procedure are discussed elsewhere [4]. Relevant geometric intensity corrections were applied to the data from oriented samples, but absorption corrections could not be applied as the sample thicknesses are not accurately known. We have confirmed, by assuming reasonable values of the sample thickness, that these corrections do not significantly change the calculated electron density profiles. However, in the absence of these corrections, we are unable to analyze these data using models II and III, due to the lack of convergence resulting from the large number of adjustable parameters in these models.

The converged values of the different parameters in the three models are given in table I, along with the crystallographic R factor. The precision of these parameters is about 0.1 %. The data from ref. [5] were used in these analyses. For powder samples of DMPC [5], models

Table I – *The values of the structural parameters obtained from the three models.*

Parameter	Model I	Model II	Model III
A (Å)	19.7	18.7	19.1
λ_1 (Å)	106.2	101.0	101.5
ψ	5.7°	9.9°	9.1°
L(Å)	41.0	37.0	37.2, 37.0(*)
$\rho_{\rm h}/\rho_{\rm m}$	1.1	0.9	1.1, 1.1(*)
f_1	-	0.6	0.7
f_2	-	0.9	0.65
$\sigma_{\rm h}$	-	4.9	4.6, 4.7(*)
$\sigma_{\rm m}$	-	13.3	9.4, 10.0(*)
w (Å)	-	2.0 (fixed)	9.2
χ^2	692.5	217.6	213.6
R	0.172	0.083	0.087

(*) Values in the shorter arm.

I, II and III give the same phases except for the faint $(0, k)$ reflections. Model III gives only a marginally better fit than model II. The values of L in the two arms are almost the same and equal to that obtained from model II. This is also true of the other parameters which are allowed to be different in the two arms. However, model III gives a slightly higher value of 0.7 for f_1. As discussed below, this factor can be accounted for in terms of the chain tilt, without resorting to the assumption of an L_α-like organization in the minor arm. The low χ^2 and R values for models II and III, and the absence of any physically unacceptable features in the electron density map (see fig. 2) indicate that these models closely represent the true structure of the system.

The electron density map of the ripple phase of DMPC, calculated with the data of ref. [5], is shown in fig. 2. The ripples clearly have a saw-tooth shape, with an offset between the two leaves of the bilayer. The simplest explanation for this offset is an average tilt of the chains along the rippling direction; such an offset cannot be expected if the tilt were in a plane normal to the rippling direction. The tilt angle ψ is found to be approximately equal to $(\gamma - \frac{\pi}{2})$. Further confirmation of the existence of an average tilt along this direction comes from the fact that the value of L is almost equal in the two arms and is comparable to twice the length of a fully stretched DMPC molecule. If it is assumed that the chains are tilted at an angle ψ with the z-axis, their tilt with respect to the local layer normal can be calculated from the shape of the ripple. Using the values of the structural parameters given in table I, the tilt angle with respect to the local layer normal turns out to be 1.6° and 34.5° in the longer and shorter arms, respectively. The tilt in the short arm is comparable to that found in the $L_{\beta'}$ phase. Since the area per molecule is inversely proportional to the cosine of this angle, a value of 0.82 is obtained for f_1. This is in very good agreement with the value of 0.77 obtained from the map for the ratio of the average electron densities in the headgroup region of the longer and shorter arms. Thus an average tilt of the chains along the rippling direction provides a consistent explanation for many features of the electron density map. This means that to a good approximation the height modulation of the bilayers along the x-axis can be described as arising from a relative sliding movement of neighboring chains, with all the chains lying in the x-z plane and tilted by a constant angle ψ with respect to the z-axis. The existence of an average chain tilt along the rippling direction breaks the reflection symmetry of the bilayer in the plane normal to it and hence can be expected to be responsible for the asymmetric ripples

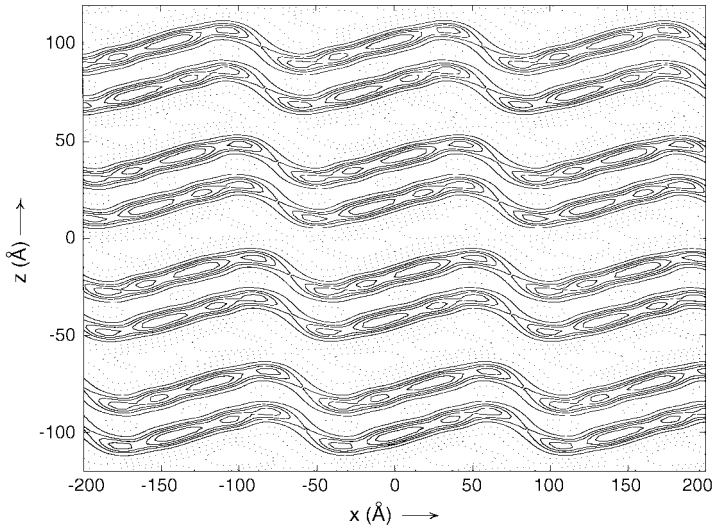

Fig. 2 – The electron density map of the ripple phase of DMPC obtained using the data from ref. [13]. $T = 18.2°$C and the volume fraction of water is 0.263. $\lambda = 141.7$ Å and $\gamma = 98.4°$. The positive (negative) contours are represented by solid (dotted) lines. The regions with positive electron density correspond to the headgroups. Note that the thickness of the bilayers is about 40 Å, whereas that of the water region is about 20 Å.

seen in this system.

We have also calculated the electron density maps of *l*-DMPC, *dl*-DMPC and POPC at different temperatures in the ripple phase, using data from oriented films. The structural features of the ripples are found to be similar to those obtained from the data of ref. [5]. The maps of the chiral and racemic DMPC samples were identical, indicating the lack of influence of molecular chirality on the ripple structure [12]. The temperature dependence of the structural parameters of the ripples in DMPC are found to be very weak, as in the case of dipalmitoyl phosphatidylcholine (DPPC) [15]. Contrary to what is observed in freeze fracture experiments [16], we find that the ripple shape has Fourier components higher than the second. Further, we do not find a significant temperature dependence of the amplitude of the ripples in contrast to what is reported in [16].

The electron density map of the ripple phase of POPC is shown in fig. 3. The ripple shape is very similar to that of DMPC. It also has a saw-tooth shape and an offset between the monolayers indicating an average tilt in the direction of rippling. In POPC, the angle γ is much larger than in DMPC, whereas the wavelength and layer spacing are comparable. Unlike

Table II – *Temperature variation of the structural parameters of the ripple phase of* POPC *at* 75% RH.

T (°C)	d (Å)	$\gamma°$	λ (Å)	A (Å)	$\frac{\lambda_1}{(\lambda-\lambda_1)}$
13.0	58.3±0.1	116±1	200±2	10±1	2.0±0.1
13.5	58.0	119	170	9	1.8
14.5	57.3	124	143	5	2.6
15.0	56.4	133	266	5	1.9

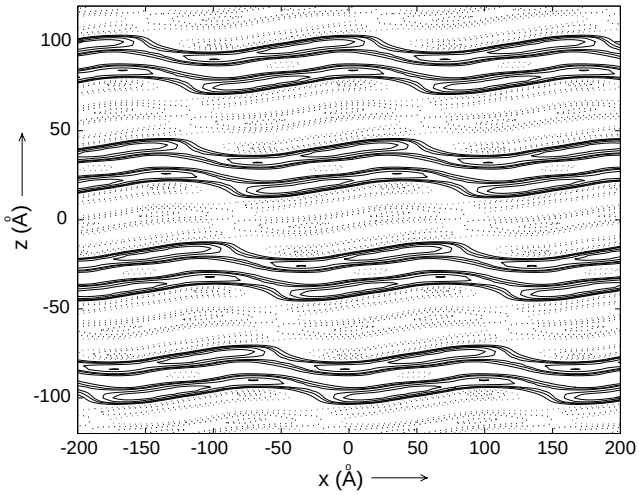

Fig. 3 – The electron density map of the ripple phase of POPC obtained using X-ray data from oriented samples. $T = 13.5°$C and RH = 75%.

those of DMPC, the structural features of the ripple phase of POPC vary significantly with temperature, as shown in table II. In the absence of absorption corrections, the fits are not as good as in the case of DMPC data of ref. [5]. As mentioned earlier, we find that the electron density profiles are insensitive to these corrections. Hence the values of the last two parameters quoted in the table are the ones estimated from the electron density maps. The layer spacing decreases slowly and γ increases steadily as temperature is increased. The ripple wavelength first decreases and then suddenly increases to a large value just below the transition. These trends are very similar to those seen in DPPC [15], but in POPC the temperature dependence is very much pronounced. The amplitude, except near the L_α transition, is about half that of DMPC. In both DMPC and POPC the ratio of the projected lengths of the major and minor arms is about 2 and is essentially insensitive to temperature. This observation further supports the view that the chain organization in the minor arm is not like that in the L_α phase.

All the freeze fracture studies of the ripple phase show ripples oriented over micrometer-sized regions [1, 15–18]. Since the chain tilt is locked to the rippling direction, this implies long-range order of the tilt direction. These experiments also show ripples oriented only along three directions, each at an angle of approximately 120° from the other two, indicating a six-fold symmetry in the underlying bilayer structure. Thus the in-plane ordering of the molecules in the bilayer is at least hexatic.

In conclusion, we have calculated the electron density maps of the ripple phase of DMPC and POPC. The shape of the ripples in these two systems are very similar, with both of them exhibiting asymmetric ripples. We have been able to establish the existence of an average chain tilt in the direction of rippling, which is probably responsible for the asymmetric ripples seen in these systems.

* * *

We thank Y. Hatwalne, K. Usha and J. F. Nagle for discussions and HKL Research Inc. for the use of their software.

REFERENCES

[1] Tardieu A., Luzzati V. and Reman F. C., *J. Mol. Biol.*, **75** (1973) 711.
[2] Smith G. S., Sirota E. B., Safinya C. R. and Clark N. A., *Phys. Rev. Lett.*, **60** (1988) 813.
[3] Janiak M. J., Small D. M. and Shipley G. G., *J. Biol. Chem.*, **254** (1979) 6068.
[4] Katsaras J. and Raghunathan V. A., *Phys. Rev. Lett.*, **74** (1995) 2022.
[5] Wack D. C. and Webb W. W., *Phys. Rev. A*, **40** (1989) 2712.
[6] Hentschel M. P. and Rustichelli F., *Phys. Rev. Lett.*, **66** (1991) 903.
[7] Yao H., Matuoka S., Tenchov B. and Hatta I., *Biophys. J.*, **59** (1991) 252.
[8] Kirchner S. and Cevc G., *Europhys. Lett.*, **28** (1994) 31.
[9] Wittebort R. J., Schmidt C. F. and Griffin R. G., *Biochemistry*, **20** (1981) 4223.
[10] Schneider M. B., Chan W. K. and Webb W. W., *Biophys. J.*, **43** (1983) 157.
[11] Lubensky T. C. and MacKintosh F. C., *Phys. Rev. Lett.*, **71** (1993) 1565; Chen C.-M., Lubensky T. C. and MacKintosh F. C., *Phys. Rev. E*, **51** (1995) 504.
[12] Sengupta K., Raghunathan V. A. and Katsaras J., *Phys. Rev. E*, **59** (1999) 2455.
[13] Sun W.-J., Tristram-Nagle S., Suter R. M. and Nagle J. F., *Proc. Natl. Acad. Sci. USA*, **93** (1996) 7008.
[14] Press W. H., Teukolsky S. A., Vellerling W. T. and Flannery B. P., *Numerical Recipes* (Cambridge University Press) 1997.
[15] Inoko Y., Mitsui T., Ohki K., Sekiya T. and Nozawa Y., *Phys. Status Solidi A*, **61** (1980) 115.
[16] Woodward J. T. and Zasadzinski J. A., *Phys. Rev. E*, **53** (1996) R3044.
[17] Luna E. J. and McConnell H. M., *Biochim. Biophys. Acta*, **466** (1977) 381.
[18] Ruppel D. and Sackmann E., *J. Phys. (Paris)*, **44** (1983) 1025.